Nanoscale Res Lett (2010) 5:1403–1407
DOI 10.1007/s11671-010-9653-7

NANO EXPRESS

A Rotating-Tip-Based Mechanical Nano-Manufacturing Process: Nanomilling

B. Arda Gozen · O. Burak Ozdoganlar

Received: 25 March 2010 / Accepted: 17 May 2010 / Published online: 25 June 2010
© The Author(s) 2010. This article is published with open access at Springerlink.com

Abstract We present a rotating-tip-based mechanical nanomanufacturing technique, referred to here as *nanomilling*. An atomic force microscopy (AFM) probe tip that is rotated at high speeds by out-of-phase motions of the axes of a three-axis piezoelectric actuator is used as the nanotool. By circumventing the high-compliance AFM beam and directly attaching the tip onto the piezoelectric actuator, a high-stiffness arrangement is realized. The feeding motions and depth prescription are provided by a nano-positioning stage. It is shown that nanomilling is capable of removing the material in the form of long curled chips, indicating shearing as the dominant material removal mechanism. Feature-size and shape control capabilities of the method are demonstrated.

Keywords Nanomilling · AFM probe · Nano-manufacturing · Nano-machining

Introduction

Tip-based creation of nano-scale features by mechanical removal has been considered since the 1990s. Motivated by the agility, geometric capability, and wide-range material applicability of mechanical removal processes, surface characterization instruments such as scanning tunneling microscopes (STMs) [1], atomic force microscopes (AFMs) [1], and nano-indenters [2] have been applied to create nano-scale features on various materials. Using AFMs at the force levels significantly higher than those used for topography measurements, simple features such as lines and pockets have been created on semiconductor [3], metal [4], and polymer/photoresist [5] surfaces through scratching or indenting. Various applications of mechanical removal at the nano-scale has been identified, including shaping of mask layers for lithography [6], fabrication of single-electron transistors (SETs) [7], and creation of Coulomb blockades, quantum point contacts, quantum nano-dots, quantum wells, and nano-wires [8–10].

Although the basic capability of AFM-based surface modification has been established, its wide-range of applicability as a viable nanomanufacturing technique has been hindered by several issues. First, the material removal mechanism is dominated by ploughing (i.e., plastic deformation) rather than shearing (i.e., removal of material in the form of a chip). This causes accumulation, rather than removal, of the material around the created features (i.e., ridge formation) [4, 6, 11]. Second, the throughput of the process is low due to the limited removal speeds, large force requirements, and associated rapid tool wear [6]. Third, the depth of removal is dictated indirectly by prescribing the force by monitoring the deflection of the relatively low-stiffness AFM cantilever. Since the material removal force depends on factors such as material (surface) properties [5], probe geometry [11], and removal conditions (e.g., removal speed) [12], the resultant removal depth cannot be well-controlled through indirect prescription of depth using force monitoring. While several approaches have been proposed to address these issues, including the use of high-stiffness cantilevers [4], vibrating cantilevers [8, 12], and vibrating workpiece [13] or diamond tips (to reduce wear) [3], significant process improvements that will make tip-based mechanical material removal as a fully controllable nanomanufacturing technique have not yet been realized.

B. A. Gozen · O. B. Ozdoganlar (✉)
Department of Mechanical Engineering,
Carnegie Mellon University, Pittsburgh, PA 15213, USA
e-mail: ozdoganlar@cmu.edu

In this letter, we present a tip-based mechanical nanomanufacturing process, referred to here as *nanomilling*, in which an AFM tip rotated at high frequencies is used as the nanotool to remove the material in a manner similar to that of the conventional milling process. The rotary motions are obtained by out-of-phase motions of the axes of a three-axis piezoelectric actuator that hosts the AFM tip. By assembling the tip directly onto the actuator, and thereby eliminating the high compliance arising from the AFM-beam connection, a high-stiffness configuration is realized. The feeding motions in three directions, which define the overall geometry, are obtained by moving the sample using a nano-positioning stage. The combined use of high-stiffness tip and nano-positioning stage enables *direct* prescription of feature depth and shape. As such, the nanomilling process has the potential to advance tip-based nanomanufacturing by enhancing the shape capability and accuracy, increasing the removal speed, and reducing the removal forces and nanotool wear.

Description of the Nanomilling Process

Two possible configurations of rotational motions of the tip (in-plane and out-of-plane) are depicted in Fig. 1a and b. These motions are obtained by supplying out-of-phase sinusoidal excitations to the axes of the piezoelectric actuator in mutually perpendicular directions. The material removal process in nanomilling is accomplished by rotating the tip in an elliptical pattern, while moving the sample along the feeding direction at a prescribed removal depth (obtained by the nanopositioning stage). For the in-plane configuration, the piezoelectric actuator is used to induce an elliptical pattern (nanotool path) to the tip within the sample-surface plane. The tip (nanotool) is represented with a circular cross-section in the top view shown in Fig. 1a. As the nanotool follows the nanotool path, the material is removed by combined feeding and rotary motions. Continuing feeding motion enables creating channels with a prescribed depth. The feeding direction can be controlled to create different feature shapes. The width of the channel can be modified by changing the diameter of the elliptical nanotool motion normal to the feeding direction.

For the out-of-plane configuration (see Fig. 1b), the nanotool is rotated in a plane perpendicular to the surface. In this case, the prescribed depth can be changed by varying the nanotool-path diameter along the sample-surface normal. Combined motion of nanotool rotation and feeding causes a portion of material (the shaded region in Fig. 1b) to be removed at each revolution of the nanotool. The amount of material removed per revolution (the size of the shaded region) depends on the prescribed feed.

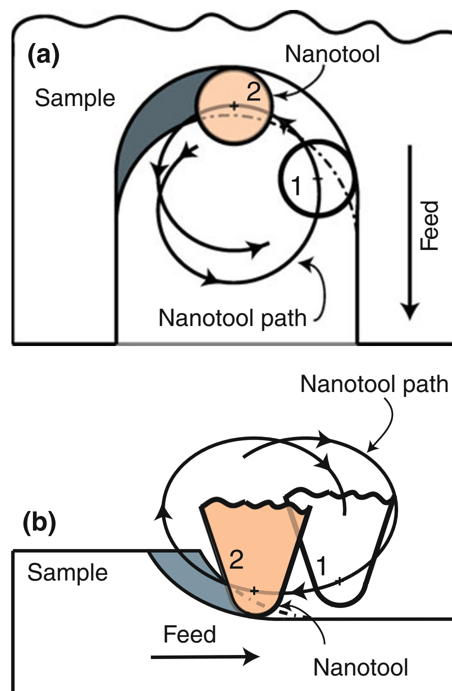

Fig. 1 Two fundamental rotational motions of the tip: **a** In-plane motion, and **b** Out-of-plane motion. The nanotool follows the indicated path to remove the material. Two instants of the cross-section of the nanotool are indicated as 1 and 2. Continued nanotool rotation will remove the *dark-shaded* portion of the sample

Experimental Setup and Procedure

To demonstrate the nanomilling process, a nanomilling testbed has been designed and constructed (see Fig. 2). An AFM tip is assembled onto an acrylic nanotool-post in a reverse configuration, where the tip is directly supported. Since the compliant AFM beam is not used as a connection element, a high-stiffness nanotool-attachment is attained. As described below, the free-standing portion of the AFM beam, along with the piezo shaker, are used for contact detection. The nanotool-post is attached to a three-axis piezoelectric actuator (Physik Instrumente L.P. PI-123.01), which provides the rotary nanotool motions. The sample is attached to a piezoelectric element (i.e., the piezo shaker) that is fixed to the nanopositioning stage (Physik Instrumente L.P. P-611.3 NanoCube®). The nanopositioning stage provides the feeding motions and prescribes the depth with 1 nm resolution and 5 nm RMS repeatability (with the closed-loop position control). The motion directions of the nanopositioning stage and the piezo actuator are characterized using a laser Doppler vibrometer (LDV) system (Polytec GmbH MSA-400) and optical reference surfaces, and are subsequently aligned using a compensation algorithm.

The nanomilling process is performed within the nanomilling testbed through the following procedure: First, the

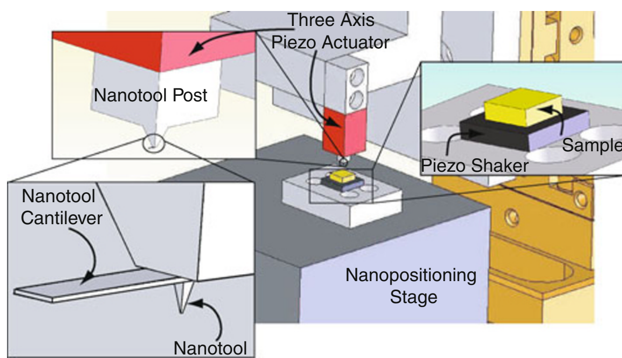

Fig. 2 A three-dimensional rendering of the nanomilling testbed, showing different components of the system

sample surface is located through a nanotool-sample contact algorithm using the nanotool cantilever. The piezo shaker placed under the sample is vibrated at the first resonant frequency of the nanotool cantilever (determined a priori through LDV measurements) with a sub-nanometer vibration amplitude. The sample is then slowly approached to the tool using the nanopositioning stage, while measuring the vibrations of the tool cantilever using the LDV. A contact between the tool and the sample surface causes a significant (an order of magnitude or more) increase in cantilever vibrations at the first resonant frequency and thus, can be detected. The (unwanted) inclination of sample surface is then measured and compensated. Second, the nanotool is rotated with selected frequency using the piezoelectric actuator. And third, the nanopositioning stage is used to prescribe the depth and feeding motions to create a particular feature.

Results and Discussion

One of the premises of the nanomilling process is the effective removal of the material mainly in the form of a chip, rather than only ploughing the material [4, 6]. To demonstrate the material removal characteristics, an SU-8 sample surface was nanomilled to create channels with 5 μm length and 100 nm depth using each of the in-plane and out-of-plane configurations (see Fig. 3). For the in-plane configuration, the nanotool was rotated using a 100 nm circular motion at 3 kHz frequency. For the out-of-plane configuration, the elliptical nanotool motion included a normal (to the surface) diameter of 40 nm and a feeding-direction diameter of 100 nm at 3 kHz frequency. As a reference, channels were also fabricated without a nanotool motion (i.e., by scratching). A commercial silicon probe tip with a pyramidal shape and 10-nm nominal tip radius was used as the nanotool. Due to the potential effect of nanotool orientation, three feeding directions were tested. It can be seen that the in-plane and out-of-plane nanotool motions

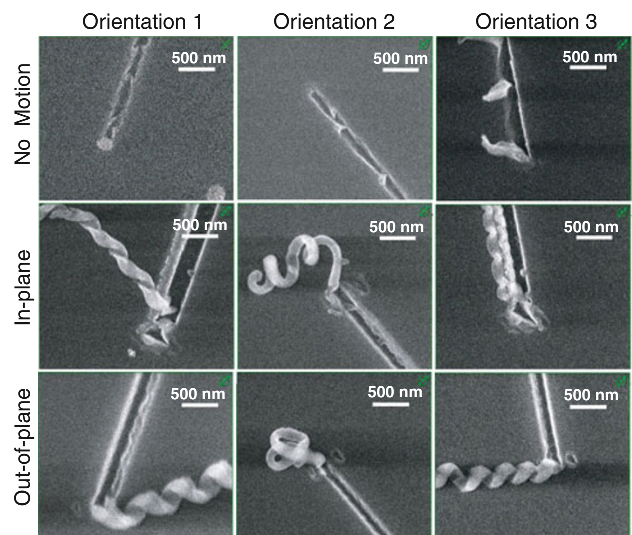

Fig. 3 SEM images of the channels created using different nanotool motions. The long and curled chips observed for the cases with nanotool motions indicate that the material removal mechanism is shearing dominated. No-motion (scratch) case does not produce chips consistently, indicating the dominance of the ploughing mechanism

facilitated material removal in the form of long, curled chips, and produced well-defined edges of the channels. The scratch (no-motion) configuration, on the other hand, did not produce chips in a consistent manner, and resulted in reduced edge definition, indicating a removal process dominated by ploughing effects.

To evaluate the capability of the nanomilling process and the testbed in *directly* prescribing the removal depth, a set of three side-by-side parallel pockets with increasing depth were created on PMMA using the in-plane configuration. Circular nanotool motions with 200 nm diameter were utilized at 3 kHz rotational frequency. To eliminate the uncertainty arising from the contact detection, the first pocket was considered as the reference. Two subsequent pockets were nanomilled by setting the depth to 50 and 100 nm, respectively, from the reference surface. Figure 4 shows the AFM image of the fabricated pockets and the associated line scan. In order to calculate the average depths, three parallel planes were fitted to the AFM scans of each created pocket, and the first plane was taken as the reference. The average depths of the second and third pockets were obtained by calculating the distances between their corresponding fitted planes and the reference plane. The standard deviation of measured surface points around the fitted planes for each pocket were also calculated. The average depth of the second and third pockets were calculated as 48.4 and 98.5 nm, respectively. The calculated standard deviation of the surface for both pockets was found to be 4 nm. The difference between the prescribed and actual depths are within the repeatability of the nanopositioning stage.

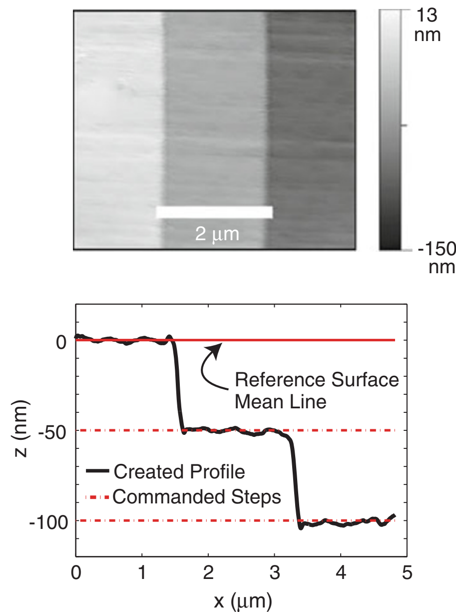

Fig. 4 An AFM image of the created depths and associated cross-sectional topography

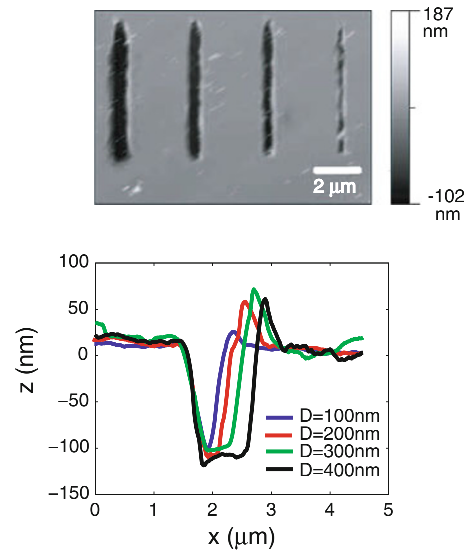

Fig. 5 An AFM image and cross-section topography of four channels with different widths, each created in a single pass using the circular in-plane motions with increasing diameter (chips around the created features are cleaned prior to imaging)

In contrast to scratching, when used in the in-plane configuration, the nanomilling process is capable of creating a range of channel widths in a single pass. To demonstrate this capability, four channels with different width value were created on SU-8, each in a single pass, by providing circular nanotool motions with 100, 200, 300, and 400 nm diameter. For each case, the rotational frequency was kept at 3 kHz, and the channel depth was set to 100 nm. An AFM image of the created channels and their cross-sectional topography data is presented in Fig. 5. Although the channel widths cannot be accurately measured due to the steep channel walls, it is seen that the width consistently increased in each successive channel.

To show the capability of nanomilling process in creating complex shapes, a set of shapes were fabricated on SU-8. Figure 6 shows SEM images of sample shapes, including a 5 μm diameter circle with 30 nm depth, fabricated by in-plane motions (see Fig. 6a); an equilateral triangle with 5 μm side length and 30 nm depth, fabricated by out-of-plane motions (see Fig. 6b); and a 4.5 μm by 4.5 μm square pocket with a 100 nm depth (see Fig. 6c) fabricated by in-plane motions.

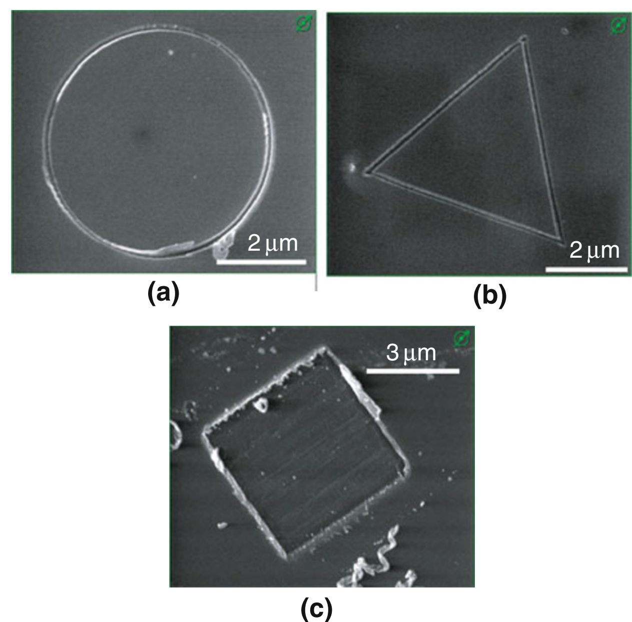

Fig. 6 Shape capability of the nanomilling process: **a** a *circular trench* nanomilled using the in-plane configuration, **b** a *triangular trench* nanomilled using the out-of-plane configuration, and **c** a *square pocket* nanomilled using the in-plane configuration

Conclusions and Future Work

In summary, this letter demonstrated the viability of a nanomanufacturing technique, *nanomilling*, that uses piezoelectrically induced rotary motions of a nanotool (AFM tip) to create nano-scale features by mechanical material removal. Two configurations of the nanomilling process that use in-plane and out-of-plane elliptical nanotool rotations were described. The components of the nanomilling testbed and the procedure for the nanomilling were then outlined. The material removal in nanomilling was observed to be dominated by shearing the material in the form a (continuous/curled) chip. It is shown that the nanomilling process possesses a high level of geometric

control, including *direct* prescription of the feature depth (due to the high nanotool-stiffness), creation of different feature widths in a single pass, and fabrication of shapes with complex geometries. It is concluded that, although further improvements are needed to increase the process efficiency and accuracy, the nanomilling process has a potential to become a controllable nanomanufacturing process for fabricating nano-scale features with complex geometries.

It is expected that, when compared to AFM scratching, the nanomilling process will yield lower forces, reduced nanotool wear, and improved feature quality. The future work will include an in-depth analysis of the effect of nanomilling parameters on the material removal mechanism, feature quality, and nanotool life. The nanomilling parameters of interest are the nanotool shape, nanomilling orientation, motion shape, frequency, and feed rate. The future work will enable identifying the optimal nanomilling parameters that will yield improved feature quality and minimum tool wear, thereby optimizing the overall throughput of the nanomilling process.

Acknowledgments This work was supported in part by the National Science Foundation award CMMI-0602401 (Ozdoganlar).

Open Access This article is distributed under the terms of the Creative Commons Attribution Noncommercial License which permits any noncommercial use, distribution, and reproduction in any medium, provided the original author(s) and source are credited.

References

1. C. Quate, Surf. Sci. **386**, 259 (1997)
2. X. Li, P. Nardi, C.-W. Back, J.-M. Kim, Y.-K. Kim, J. Micromech. Microeng. **15**, 551 (2005)
3. N. Kawasegi, N. Takano, D. Oka, N.Morita, S. Yamada, K. Kanda, S. Takano, T. Obata, K. Ashida, J. Manuf. Sci. Eng. Trans. ASME **128**, 723 (2006)
4. H. Goebel, P. von Blanckenhagen, J. Vac. Sci. Technol. B Microelectron. Process. Phenom. **13**, 1247 (1995)
5. X. Jin, W. Unertl, Appl. Phys. Lett. **61**, 657 (1992)
6. A. Notargiacomo, V. Foglietti, E. Cianci, G. Capellini, M. Adami, P. Faraci, F. Evangelisti, C. Nicolini, Nanotechnology **10**, 458 (1999)
7. H. Schumacher, U. Keyser, U. Zeitler, R. Haug, K. Eberl, Phys. E Low Dimens. Syst. Nanostruct. **6**, 860 (2000).
8. M. Versen, B. Klehn, U. Kunze, D. Reuter, A. Wieck, Ultramicroscopy **82**, 159 (2000)
9. U. Keyser, M. Paesler, U. Zeitler, R. Haug, K. Eberl, Phys. E Low Dimens. Syst. Nanostruct. **13**, 1155 (2002)
10. S. Hu, A. Hamidi, S. Altmeyer, T. Koster, B. Spangenberg, H. Kurz, J. Vac. Sci. Technol. B Microelectron. Process. Phenom. **16**, 2822 (1998)
11. Y. Ichida, Y. Morimoto, R. Sato, M. Murakami (Cambridge, MA 02139, United States, 2003), pp. 534–537
12. C. Hyon, S. Choi, S. Hwang, D. Ahn, Y. Kim, E. Kim, Appl. Phys. Lett. **75**, 292 (1999)
13. F. Iwata, M. Kawaguchi, H. Aoyama, A. Sasaki, Thin Solid Films **302**, 122 (1997)